



# Dependence of oxygen desorption kinetics on processing methods of SrCoO<sub>2.5</sub>

ASWATHY M NARAYANAN\*  and ARUN M UMARJI

Materials Research Centre, Indian Institute of Science, Bengaluru 560012, India

\*Author for correspondence (aswathyn@iisc.ac.in)

MS received 13 June 2020; accepted 17 September 2020

**Abstract.** The effect of processing methods on oxygen storage and exchange kinetics of brownmillerite (BM) SrCoO<sub>2.5</sub> is compared in terms of their reversible oxygen incorporation and desorption kinetics. BM SrCoO<sub>2.5</sub> was synthesized through two different methods; solid-state synthesis and the nitrate–citrate gel method, both followed by Al foil pad quenching. Oxygen storage characteristics of synthesized samples were analysed using a home-built volumetric set-up. The maximum oxygenation achievable for BM SrCoO<sub>2.5</sub> under prevailing conditions of O<sub>2</sub> partial pressure (16 bar O<sub>2</sub>), temperature (673 K) and time (1 h) was unaltered, regardless of the synthesis method. Oxygen exchange kinetics of desorption was faster in the nitrate–citrate synthesized sample than in the solid-state synthesized sample. The kinetics of desorption correlated with the crystallite and particle sizes of the samples. The mechanism of desorption follows nucleation and growth model for nitrate–citrate synthesized sample, while it follows contracting sphere model for solid-state synthesized sample.

**Keywords.** Oxygen ion diffusion; oxygen non-stoichiometry; mixed ion electron conductor; perovskite oxide; desorption kinetics.

## 1. Introduction

Transition metal oxides have versatile applications in gas sensing, catalysis, cathodes of solid oxide fuel cell and oxygen separation membranes due to the presence of metals with variable oxidation states [1–5]. These metal oxides can have variable oxygen non-stoichiometry with respect to the surrounding temperature and oxygen partial pressure [6–10]. Certain metal oxides even find applications as oxygen sorbents for oxygen storage, separation and enrichment due to its fast response to the changes in ambient oxygen partial pressure and/or temperature [8,9,11–13]. A notable material explored for such applications is brownmillerite (BM) SrCoO<sub>2.5</sub> [11,14,15] because of its highest theoretical oxygen intake/release per gram of the material among the other reported oxide materials [11].

Oxygen sorbent transition metal oxide absorbs oxygen from surrounding air atmosphere to fill its lattice oxygen vacancies at a specified temperature range and releases oxygen at a lower oxygen pressure and/or different temperature range [5,12]. This necessitates the presence of a large number of oxygen vacancies in the structure, faster oxygen surface exchange and oxide ion diffusion inside the lattice [5,16]. Different strategies have been used for tuning these parameters, including aliovalent substitution, forming composites of two materials with one or more of these best properties and using equilibrium/non-equilibrium synthesis

methods [17–22]. A large variety of methods have been adopted in literature for the synthesis of mixed oxide ceramics [23–27]. The phase purity, morphology and particle size can be tuned by selecting suitable synthesis methods, which in turn alter the physico-chemical properties [16,22,24,28]. The most common methods employed for the synthesis of oxide materials include solid-state reaction [23] and wet chemistry methods like co-precipitation [25], solution combustion synthesis [29] and sol–gel method [24–27].

Conventionally, solid-state reaction (or heat and beat method) between the corresponding metal oxides is widely used for the synthesis of oxide ceramics in large scale because of its simplicity and low manufacturing cost [23]. The relatively high temperatures required to increase solid-state reaction kinetics usually result in low homogeneity, uncontrolled and large particles with a low surface area. To obtain homogeneous materials via solid-state reaction, maximizing the surface area of the reactants so as to improve the reaction rate is considered [23,24]. Also, oxysalts of the metals rather than oxides are preferred as precursor materials. These oxysalts are usually decomposed *in situ* to obtain high surface area oxides, which react further to form the required phase [23]. Another commonly employed method is the sol–gel process, which involves the hydrolysis and polymerization of heterometallic alkoxide precursors to obtain a gel, which is further fired to acquire

the required oxide [24,27]. The organic part of the alkoxide and pH conditions are varied for the formation of homogeneous gel, which in turn gives a homogeneous oxide product [27].

Bezducka *et al* [30] synthesized BM SrCoO<sub>2.5</sub> using four different methods followed by liquid nitrogen quenching and attempted to oxygenate it by electrochemical technique. They found that the samples differed in their density, particle size and homogeneity with varied synthesis methods. The sample with 80% density and 1–3 μm particle size was found to be optimum for electrochemical oxidation. In this work, the oxygen intake/release properties of BM SrCoO<sub>2.5</sub> synthesized through solid-state reaction and the sol–gel method have been compared. As BM phase is metastable, the phase stabilization was performed by quenching using a heated Al foil pad for both samples. We further compare the reversible oxygen intake and desorption kinetics of these two samples considering the differences in particle and crystallite sizes.

## 2. Materials and methods

### 2.1 Synthesis

The BM SrCoO<sub>2.5</sub> was synthesized through two different methods.

**2.1a Solid-state synthesis:** Stoichiometric amounts of SrCO<sub>3</sub> (SD Fine Chemicals, 99%) and CoC<sub>2</sub>O<sub>4</sub>·2H<sub>2</sub>O [31] were weighed, wet mixed with acetone and calcined at 1173 K for 2 h. The obtained black powder was ground, mixed well and heat treated for 5.5 h with one intermediate grinding to complete the reaction. Obtained powder was made into a pellet of 10 mm diameter using a cold uniaxial press. The pellet was soaked at 523 K for 3 h to remove the binder and heat-treated at 1223 K for 6 h with one intermediate grinding. The pellet was quenched to room temperature from 1223 K using a pad of heated multilayer Al foil pre-heated at about 373–473 K to stabilize the intact pellet of high temperature BM phase. The sample obtained through this method is coded as SC-SSS throughout this work.

**2.1b Nitrate–citrate gel method:** Stoichiometric amounts of SrCO<sub>3</sub>, CoC<sub>2</sub>O<sub>4</sub>·2H<sub>2</sub>O and citric acid (1:1:3 ratio) were dissolved in hot dilute nitric acid and introduced to 773 K in a preheated furnace. Water evaporation takes place within few minutes and the formed gel undergoes auto-combustion to give a voluminous black powder. The obtained black powder was mixed well and calcined at 1173 K for 8 h. It was made into a pellet of 10 mm diameter using a cold uniaxial press. The pellet was quenched to room temperature as above after sintering at 1223 K for 4 h. The sample obtained through this method is coded as SC-NC throughout this work.

### 2.2 Characterizations

Phase purity of the samples were analysed using X-ray diffraction (XRD, PANalytical X'Pert Pro, Cu Kα). The diffraction pattern was collected in the angular range 10–90° with a step size of 0.02° for 20 min for phase purity analysis. Data collected in the same 2θ range and step size for 1 h was used for Rietveld profile refinement to calculate the lattice parameters using GSAS II software [32]. The instrumental profile parameters for the refinement was obtained by refining data of standard Si sample with minimum crystallite size and strain broadening. The profile shape was calculated using a pseudo-voigt profile function and the irregular background was fitted using manually selected background points and with Chebyshev function.

Morphology of the samples were analysed using a field emission scanning electron microscope (FESEM, FEI INSPECT F50) equipped with an energy dispersive spectrometer (EDS, Oxford Instruments) for elemental analysis. The average particle size of the samples were calculated using Image-J Software [33]. Density of the samples were measured using Archimedes method and was converted to relative density (% theoretical density) comparing it with that observed from structural data.

Oxygen intake/release studies of the differently synthesized samples were performed in a home-built volumetric apparatus reported elsewhere [14]. In a typical experiment, pieces of the as-synthesized BM sample was pressurized with 16 bar O<sub>2</sub> pressure and heated to 648/673 K with a heating rate of 6 K min<sup>-1</sup>. It was soaked at that temperature for 1 h and cooled back to room temperature in the same oxygen pressure. A known amount of this oxygenated sample was heated to 693 K with a heating rate of 6 K min<sup>-1</sup> under reduced oxygen pressure where oxygen desorption takes place. The volume of oxygen which is reversibly incorporated into the material is calculated using the ideal gas equation,  $PV = nRT$ . Further, isothermal desorption kinetics of the absorbed samples were studied as a function of desorption temperature. Desorption was performed isothermally at 673, 693 and 723 K as a function of time for SC-SSS and SC-NC samples absorbed at 673 K/1 h/16 O<sub>2</sub>.

Oxygen absorption and release was confirmed by XRD and iodometric titration of as-synthesized, absorbed and desorbed samples. A known amount of the sample (~30 mg) was dissolved in dilute hydrochloric acid containing an excess of potassium iodide. The evolved iodine from the reaction is titrated against standardized sodium thiosulphate solution with freshly prepared starch solution as an indicator towards the end of the titration.

DC electrical conductivities of the samples were measured using four probe Van der Pauw technique [34] on a disc-shaped pellet of 10 mm diameter and ≈2 mm thickness. Measurements were conducted in the ambient air, flowing nitrogen and flowing oxygen atmospheres from room temperature to 715 K. Electrical contacts were made

between the sample and platinum leads by applying silver paste (FERRO LAQUE L200).

Linear thermal expansion of as-synthesized and absorbed bar-shaped ( $10 \times 2 \times 2 \text{ mm}^3$ ) samples were measured using a differential dilatometer (DIL 802, TA Instruments) with respect to alumina reference in the ambient air atmosphere from room temperature to 1000 K.

### 3. Results and discussion

#### 3.1 Structural characterization

Figure 1a, b shows the refined XRD patterns of the BM  $\text{SrCoO}_{2.5}$  samples, SC-SSS and SC-NC, respectively. Both samples are phase pure and the XRD pattern can be indexed considering a unit cell based on *Ima2* space group [35]. The refined XRD patterns show good fit between measured and calculated profiles. The lattice parameters calculated are given in table 1. Williamson-Hall analysis was carried out to compare the crystallite sizes of the samples obtained through different methods (figure 2). Peaks in the  $2\theta$  range  $30\text{--}50^\circ$  were selected for plotting Williamson-Hall plot. Peaks were de-convoluted assuming Gaussian profile shape. The full-width at half-maxima (FWHM) were corrected by subtracting the FWHM of the standard Si sample ( $\beta_{\text{actual}} = (\beta_{\text{meas}}^2 - \beta_{\text{inst}}^2)^{1/2}$ ). The obtained crystallite size and strain values are tabulated in table 1. The crystallite size of the SC-NC sample was smaller than that of the SC-SSS sample, mainly due to the difference in heat-treatment during the synthesis of these samples (section 2.1).

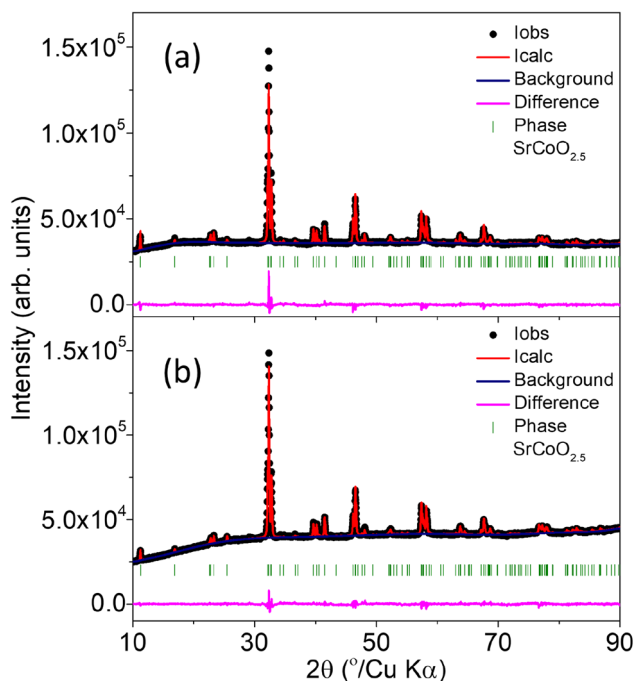


**Figure 1.** The refined XRD pattern of BM  $\text{SrCoO}_{2.5}$  samples: (a) SC-SSS and (b) SC-NC.

#### 3.2 Morphological characterization

SEM micrographs and energy dispersive spectra (EDS) of the SC-SSS and SC-NC samples are given in figure 3a–d. Both SC-NC and SC-SSS show moderately interconnected globular particles with porous microstructure. The average particle size was slightly different (figure 3a and b and table 1), SC-SSS sample had bigger particle size than SC-NC sample. EDS shows the presence of Sr, Co and O in both samples (figure 3c and d).

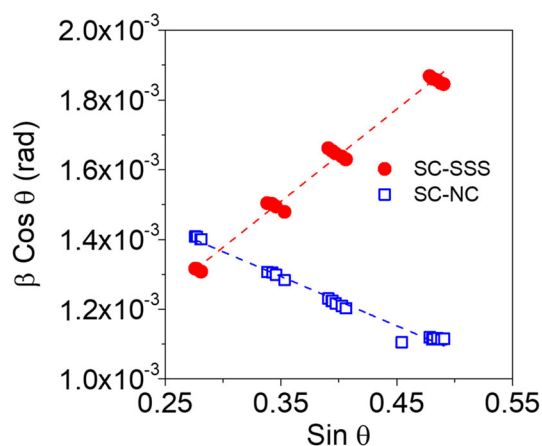
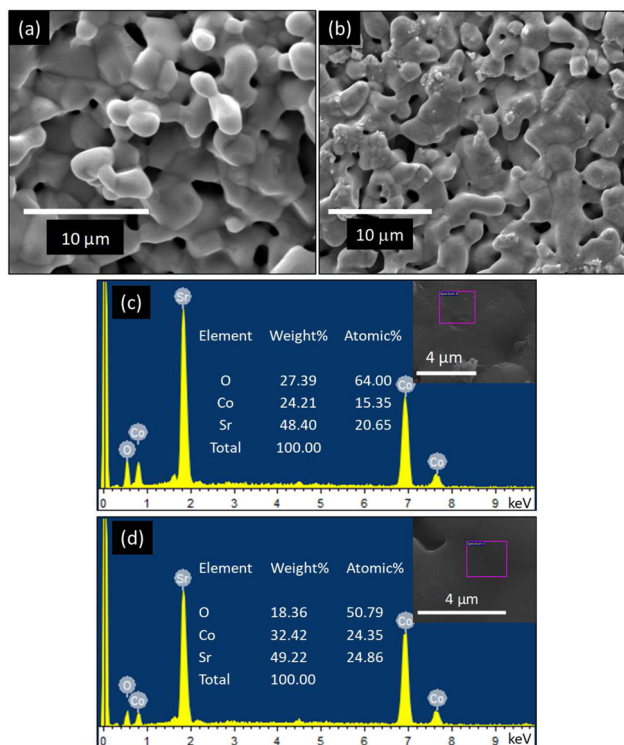
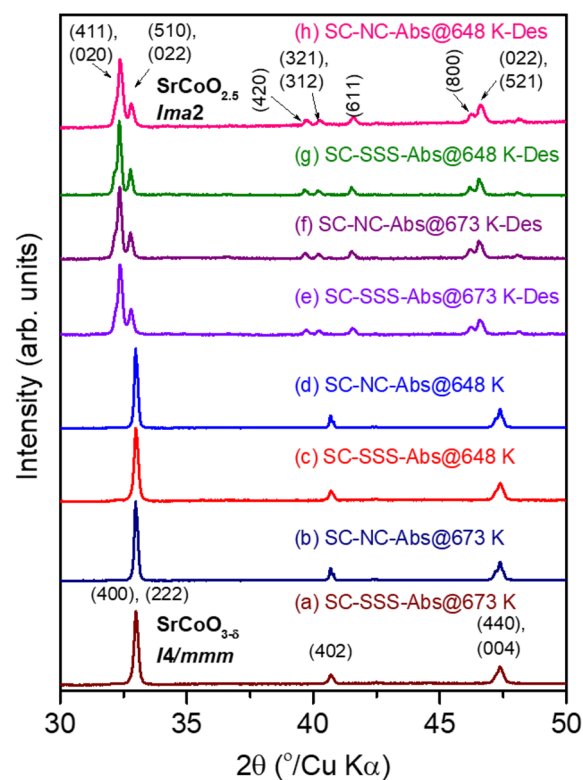
#### 3.3 Oxygen storage measurements

Oxygen absorption and desorption studies were performed with the samples as mentioned in section 2.2. Absorption was conducted with SC-SSS and SC-NC samples at 673 K by pressurizing with 16 bar of  $\text{O}_2$  and the desorption was carried out as a function of temperature at a reduced pressure. The XRD patterns of absorbed SC-SSS and SC-NC samples are given in figure 4a and b. It can be seen from the figure that both the samples have been converted to perovskite phase. A peak splitting was observed for the peak near  $47.4^\circ$ , indicating a reduced symmetry compared to the true perovskite phase. Thus, *I4/mmm* space group [36] was used to index the XRD pattern of the absorbed samples. Rietveld profile refinement was carried out to obtain lattice parameters and the formula unit cell volumes are tabulated in table 2. Both the samples show a reduction in cell volume compared to the as-synthesized samples indicating oxygen absorption. There is no significant change observed in the normalized cell volume for the two samples, indicating a similar oxygen content. The oxygen content obtained from iodometric titration (table 2) implies the same. Because the as-synthesized samples were found to differ in their crystallite and particle sizes, the reversible oxygen absorption may also differ at a lower temperature. Thus, absorption was carried out at a lower temperature, 648 K. XRD patterns of the absorbed samples (figure 4c and d) show that it has converted to perovskite phase.

The desorption curves of absorbed SC-SSS and SC-NC samples are given in figure 5. The volume of evolved oxygen starts to increase above a certain temperature as shown in the figure, it reaches a maximum value and remains constant when it is cooled down to room temperature. The total volume of desorbed oxygen was found to be similar in both SC-SSS and SC-NC samples absorbed at 673 K as well as 648 K (figure 5 and table 2). The oxygen intake was slightly lower for the samples absorbed at a lower temperature (figure 5 and table 2). The maximum reversible oxygen intake matches with the one reported earlier for a similar sample synthesized through solution combustion synthesis [14]. This reflects the maximum oxygenation achievable for BM  $\text{SrCoO}_{2.5}$  at the absorption conditions to be constant irrespective of the synthesis method employed. XRD patterns of the sample after

**Table 1.** Structural parameters of the BM SrCoO<sub>2.5</sub> samples from Rietveld profile refinement, XRD and SEM.

Sample code	Lattice parameters (Å)			Cell volume (Å <sup>3</sup> )	Cell volume per formula unit (Å <sup>3</sup> )	Crystallite size (μm) (XRD)	Strain (XRD)	Relative density (%)	Average particle size (μm) (SEM)
	<i>a</i>	<i>b</i>	<i>c</i>						
SC-SSS	15.726 (5)	5.569 (2)	5.464 (7)	478.526 (14)	59.815 (2)	0.24	+0.003	85–90	3.0 ± 0.8
SC-NC	15.724 (4)	5.568 (8)	5.464 (8)	478.379 (20)	59.797 (3)	0.08	−0.001	90–95	2.0 ± 0.8

**Figure 2.** W-H plots for SC-SSS and SC-NC samples. Dashed lines indicate fit to the data points.**Figure 3.** Scanning electron micrographs of BM SrCoO<sub>2.5</sub> samples: (a) SC-SSS and (b) SC-NC. EDS of samples: (c) SC-SSS and (d) SC-NC. Elemental composition as obtained from EDS is also shown.**Figure 4.** Comparison of XRD patterns of absorbed and desorbed samples: (a) SC-SSS absorbed at 673 K, (b) SC-NC absorbed at 673 K, (c) SC-SSS absorbed at 648 K and (d) SC-NC absorbed at 648 K. Desorbed after absorption at 673 K: (e) SC-SSS and (f) SC-NC. Desorbed after absorption at 648 K: (g) SC-SSS and (h) SC-NC.

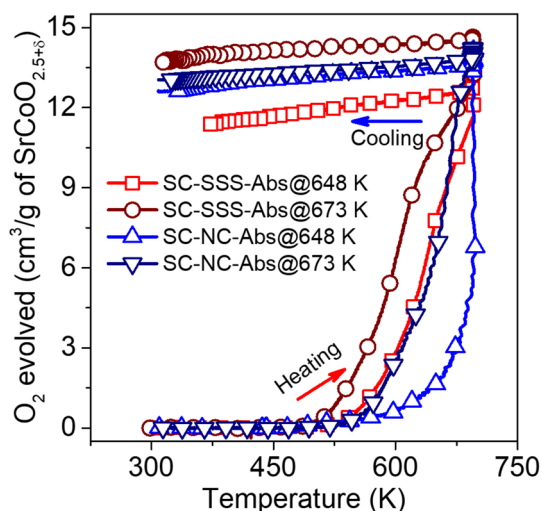
desorption indicates a reversible structural change, where the perovskite phase converts back to the BM phase after desorption (figure 4e and f).

### 3.4 Kinetics of O<sub>2</sub> desorption

In an oxygen separation/enrichment point of view, an oxygen sorbent will be efficient only if it gives out the absorbed oxygen as fast as possible by an appropriate heat-treatment. The kinetics of oxygen evolution of oxygenated BM SrCoO<sub>2.5</sub> was analysed to understand the effect of synthesis method if any, on oxygen desorption. For this, isothermal desorption of the samples absorbed at

**Table 2.** Comparison of oxygen evolved and delta values from desorption experiments and iodometric titration for SC-SSS and SC-NC samples. Cell volume per formula unit of the absorbed samples are also given.

Sample code and absorption temperature (K)	Desorption experiment		Iodometric titration				Cell volume per formula unit ( $\text{\AA}^3$ )
	$\text{O}_2$ evolved ( $\text{cm}^3 \text{g}^{-1}$ of $\text{SrCoO}_{2.5+\delta}$ )	Delta ( $\delta$ )	Oxygen content			Delta ( $\delta$ )	
			As-synthesized	Absorbed	Desorbed		
SC-SSS and 673 K	$14.5 \pm 0.5$	0.24	$2.38 \pm 0.01$	$2.67 \pm 0.02$	$2.46 \pm 0.01$	0.21	56.490 (1)
SC-NC and 673 K	$13.5 \pm 0.6$	0.22	$2.43 \pm 0.01$	$2.69 \pm 0.02$	$2.43 \pm 0.01$	0.26	56.571 (8)
SC-SSS and 648 K	$13.1 \pm 0.5$	0.22	$2.38 \pm 0.01$	$2.62 \pm 0.01$	$2.45 \pm 0.01$	0.17	56.644 (7)
SC-NC and 648 K	$13.3 \pm 0.3$	0.22	$2.43 \pm 0.01$	$2.68 \pm 0.02$	$2.43 \pm 0.01$	0.25	56.600 (2)

**Figure 5.** Desorption curves of samples SC-SSS and SC-NC absorbed at 648 and 673 K for 1 h in 16 bar  $\text{O}_2$ .

673 K/16 bar  $\text{O}_2$ /1 h was carried out at three different temperatures, 673, 693 and 723 K. The normalized isothermal desorption curves (or the extent of conversion,  $\alpha$ ) of SC-SSS and SC-NC samples as a function of time are given in figure 6a and b, respectively. Normalization was carried out by dividing the whole curve of evolved oxygen with its maximum value. It can be seen from the figures that the desorption becomes faster for both samples as temperature increases. However, the time scale for desorption was observed to be different for SC-SSS and SC-NC samples (figure 6a and b), SC-SSS samples show a slower desorption compared to SC-NC samples at the same temperature.

The mechanism of reduction of  $\text{SrCoO}_{2.5+\delta}$  can be explained using a derivative of the extent of conversion ( $d\alpha/dt$ ) vs. the extent of conversion curve. If  $d\alpha/dt$  increases and then decreases with an increase in extent of conversion, the mechanism of desorption follows nucleation and growth. If  $d\alpha/dt$  increases with an increase in  $\alpha$ , the mechanism of desorption follows the contracting sphere model [11,37]. It can be seen from the  $\alpha$  vs.  $d\alpha/dt$  curves (figure 6c) that the

mechanism of desorption for SC-SSS samples can be explained using the contracting sphere model while that of SC-NC follows the nucleation and growth model.

The change in mechanism can be understood by considering the available reaction sites in both the samples. Sample SC-NC having smaller particle and crystallite size might have a greater number of grain boundaries, where the oxygen surface exchange reaction could be faster. This indicates a greater number of nucleation sites for SC-NC sample compared to the SC-SSS sample, thus following nucleation and growth model of desorption. In contrast, SC-SSS sample has bigger particles and thereby a lower number of active surface sites, which get nucleated fast covering the whole active surface with the reduced form ( $\text{SrCoO}_{2.5}$ ). This apparently alters the reduction mechanism to contracting sphere model.

Further analysis of the desorption kinetics was performed by fitting the extent of conversion vs. time curve using a least square fitting method, assuming a first-order reaction. Only one exponential term was enough to fit the curve at all three temperatures for the SC-SSS sample, whereas two terms were required for the sample SC-NC. Two terms can be considered as related to oxygen surface exchange and oxide ion conduction in SC-NC whereas in SC-SSS sample, oxide ion conduction can be perceived as the rate limiting step. The fitting results are shown in table 3 and the red lines in figure 6a and b indicate the best fit to the data. Using the relaxation times ( $\tau_1$  and  $\tau_2$ ) rate constants ( $k_1$  and  $k_2$ ), respectively, were calculated. The rate constants follow an Arrhenius relation with temperature as shown in figure 6d. Activation energies calculated from the slope of curves are tabulated in table 3.

### 3.5 Electrical conductivity measurements

The changes in oxygen non-stoichiometry of the oxide material with partial pressure of  $\text{O}_2$  changes the carrier concentration and thereby its electrical conductivity. Non-stoichiometric oxides can have electrons, holes as well as

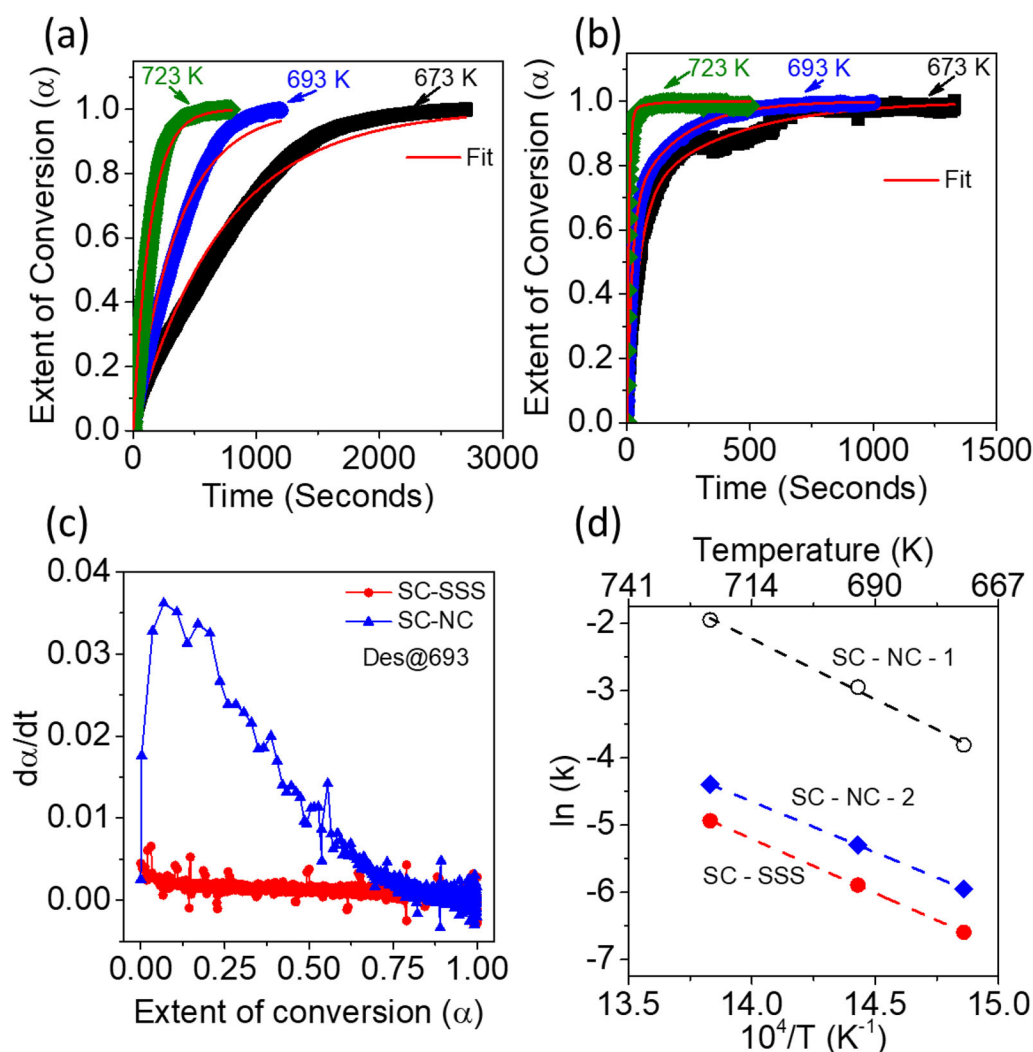
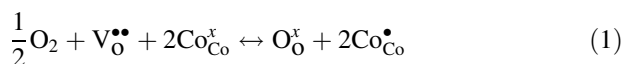


**Figure 6.** Time vs. the extent of conversion ( $\alpha$ ) curves for isothermal desorptions at 673, 693 and 723 K for samples: (a) SC-SSS and (b) SC-NC. (c)  $\alpha$  vs.  $d\alpha/dt$  for the samples SC-SSS and SC-NC desorbed at 693 K. (d) Arrhenius plots of rate constants for SC-SSS and SC-NC.

oxide ions as charge carriers as per defect reactions in equations (1) and (2). Here Kröger-Vink notations,  $V_{O}^{\bullet\bullet}$ ,  $Co_{Co}^x$ ,  $O_{O}^x$ ,  $Co_{Co}^{\bullet}$  and  $Co'_{Co}$  denotes a vacancy of oxygen,  $Co^{3+}$  in a regular lattice site, an oxide ion in its lattice site,  $Co^{4+}$  in  $Co^{3+}$  lattice site (hole) and  $Co^{2+}$  in  $Co^{3+}$  lattice site (excess electrons), respectively. The excess electrons are produced by Co ion charge-disproportionation reaction (equation 2) at high temperatures and low oxygen partial pressures [38].



The concentration of these charge carriers usually depends on the ambient oxygen partial pressure and temperature. Thus, the variation of electrical conductivity ( $\sigma$ )

with the temperature of SC-SSS and SC-NC samples were measured in the ambient air, flowing nitrogen and flowing oxygen atmospheres (figure 7a). Total conductivity increases with an increase in temperature indicating semiconducting behaviour for both SC-SSS and SC-NC samples in all three atmospheres. Both SC-SSS and SC-NC samples show similar behaviour in conductivity variation with temperature in the ambient air atmosphere. The room temperature electrical conductivity was found to be 0.01 and 0.02  $S\ cm^{-1}$  for SC-SSS and SC-NC samples, respectively, in the ambient air atmosphere, which increases to a maximum value of 10 and 12  $S\ cm^{-1}$  at 715 K.

Conductivity in  $N_2$  as well as in  $O_2$  was found to be higher than that in the air for both the samples. Further, a sharp increase in conductivity at  $\approx 600$  K was observed for both the samples in all three atmospheres. The increase in conductivity in air and oxygen atmospheres might be due to

**Table 3.** Fitting results for desorption kinetics study for SC-SSS and SC-NC samples.

Desorption temperature (K)	Equation	A1	$\tau_1$ (s)	A2	$\tau_2$ (s)
SC-NC					
673	$y = A1 \times \exp(-t/\tau_1) + A2 \times \exp(-t/\tau_2) + 1$	-0.69 (8)	45 (1)	-0.31 (4)	383 (5)
693		-0.66 (6)	19 (1)	-0.34 (3)	199 (1)
723		-0.97 (1)	7 (1)	-0.03 (5)	81 (15)
Activation energy (eV)		1.55		1.30	
SC-SSS					
673	$y = 1 - \exp(-t/\tau_2)$				731 (2)
693					362 (2)
723					139 (1)
Activation energy (eV)					1.39

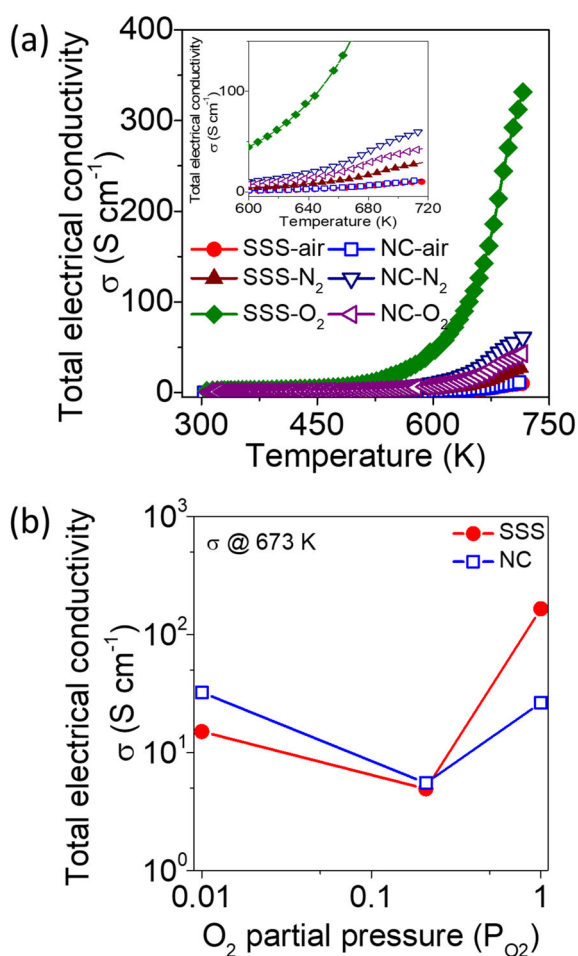


**Figure 7.** The electrical conductivity of the samples SC-SSS and SC-NC (a) in the ambient air, N<sub>2</sub> and O<sub>2</sub> atmospheres as a function of temperature and (b) as a function of partial pressure of O<sub>2</sub> at 673 K.

oxygen intake, whereby it increases both *p*-type as well as oxide ion conductivity. It should be noted that even though the total conductivity includes contribution from oxide ion conductivity, it might be negligible, of the order of

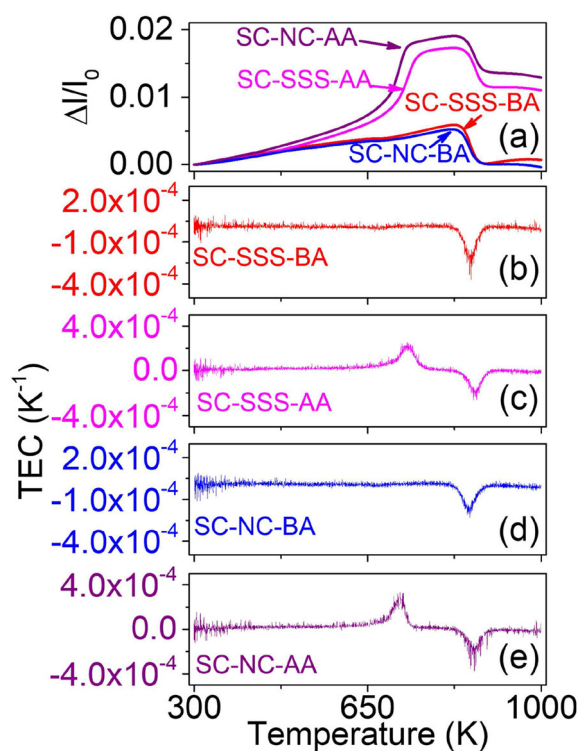


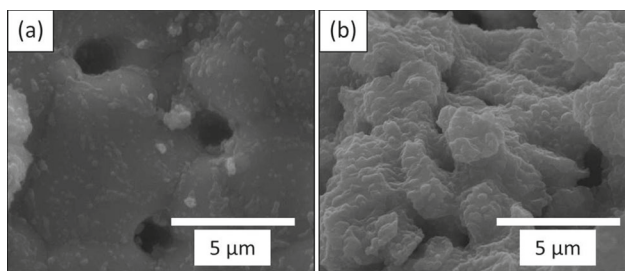
**Figure 8.** For the samples SC-SSS, SC-NC and those absorbed in 16 bar O<sub>2</sub> at 673 K for 1 h: (a) linear thermal expansion ( $\Delta l/l_0$ ) and (b–e) variation of thermal expansion coefficients (TEC) with temperature. BA = before absorption, AA = after absorption.

10<sup>-2</sup> S cm<sup>-1</sup> or less. In nitrogen atmosphere, reduction of the oxide and Co-ion disproportionation might be taking place above 600 K increasing the electron concentration and *n*-type conductivity.

Electrical conductivity of SC-SSS and SC-NC samples at 673 K (absorption temperature) in all three atmospheres were extracted from figure 7a and is plotted against the approximate oxygen partial pressure inside the measurement chamber (figure 7b). In N<sub>2</sub>,  $\sigma$  was found to be higher for SC-NC than SC-SSS while in O<sub>2</sub>,  $\sigma$  was higher for

**Table 4.** Thermal expansion coefficients of the as-synthesized and absorbed SC-SSS and SC-NC samples.

Sample code	Thermal expansion coefficient (TEC $\times 10^6$ K <sup>-1</sup> )		
	As-synthesized ( $T < 750$ K)	Absorbed ( $T < 650$ K)	Absorbed ( $750$ K $< T < 830$ K)
SC-SSS	10.7	20.2	8.8
SC-NC	9.9	20.9	12.7

**Figure 9.** Scanning electron micrographs of (a) the SC-SSS and (b) the SC-NC samples after desorption.

SC-SSS than SC-NC. The same behaviour was observed at all other measured temperatures (300–715 K). Opposite behaviour of these samples' total electrical conductivity necessarily indicates a change in the conduction mechanism with the change in surrounding atmosphere, pointing towards a  $p$  to  $n$  transition with lowering oxygen partial pressure.

For cobalt-based microcrystalline ceramics of predominant electronic conductivity, increasing the grain size showed positive effects in ionic conductivity [16]. Similarly, in our case, the SC-SSS sample with higher crystallite and particle size showed a higher total electrical conductivity in the oxygen atmosphere than the SC-NC sample. This may be because of the higher ionic contribution to conductivity for SC-SSS samples above the absorption temperature due to its bigger particle size. In contrast, the electrical conductivity of the SC-NC sample was found to be higher than the SC-SSS sample in nitrogen atmosphere, may be due to a fast oxygen release as observed from the desorption kinetics study (section 3.4). Faster oxygen release indicates a greater number of electrons created increasing the total electrical conductivity.

### 3.6 Thermal expansion measurements

The oxygenated samples show a reduced unit cell volume compared to the as-synthesized samples (table 1 and table 2). This can give rise to a difference in thermal expansion between as-synthesized and oxygenated samples, which affects the reversible oxygen intake on cyclic oxidation/reduction treatments. Also, BM SrCoO<sub>2.5</sub>

synthesized through different methods may vary in their thermal expansion coefficients because of their differences in density. Hence, the linear expansion with temperature of the as-synthesized and absorbed samples were measured.

Linear thermal expansion ( $\Delta l/l_0$ ) and the variation of thermal expansion coefficients (TEC) with temperature of as-synthesized as well as absorbed SC-SSS and SC-NC samples are given in figure 8a–e. The thermal expansion behaviour of both the as-synthesized samples were observed to be similar. Thermal expansion coefficients are tabulated in table 4, showing no significant difference between the studied samples. Above 830 K, a sharp change in expansion is observed for both the samples, where they get converted to the hexagonal phase of strontium cobaltite (Sr<sub>6</sub>Co<sub>5</sub>O<sub>15</sub>). Oxygenated samples show a higher thermal expansion coefficient than as-synthesized samples, owing to the chemical expansion due to oxygen release. Further, the absorbed samples show a drastic change in expansion behaviour due to oxygen evolution above 650 K. These samples as well get converted to hexagonal phase above 830 K.

### 3.7 Morphology after desorption

The morphology of the samples after desorption is assessed for any changes after oxygen intake/release measurements (figure 9a and b). Small surface patches were seen on the surface of the SC-SSS and SC-NC samples after oxygen intake/release studies, which may be due to the formation of surface secondary phases [11,39,40].

## 4. Conclusions

Effect of synthesis methods on the oxygen exchange kinetics of BM SrCoO<sub>2.5</sub> was explored. BM SrCoO<sub>2.5</sub> was synthesized through two different methods, solid-state reaction and nitrate–citrate gel method. Oxygen absorption/desorption characteristics of these samples were analysed using a home-built volumetric set-up. Irrespective of the synthesis method used, the total oxygen holding capacity was found to be same for all three BM SrCoO<sub>2.5</sub> samples. The sample SC-SSS releases oxygen at a slower rate compared to SC-NC and follows contracting sphere model



desorption, whereas SC-NC sample follows nucleation and growth kinetics for oxygen desorption.

### Acknowledgements

We acknowledge Supercomputer Education and Research Centre (SERC), IISc, for the access of LabVIEW 7 program. AMN acknowledges Council of Scientific and Industrial Research (CSIR), Government of India, for the financial support in the form of Junior and Senior Research Fellowship. We also acknowledge FIST for providing funding for XRD, SEM and Dilatometry facilities.

### References

- [1] Fergus J W 2007 *Sens. Actuators B Chem.* **123** 1169
- [2] Montini T, Melchionna M, Monai M and Fornasiero P 2016 *Chem. Rev.* **116** 5987
- [3] Kim J-H and Manthiram A 2008 *J. Electrochem. Soc.* **155** B385
- [4] Badwal S P S and Ciacchi F T 2001 *Adv. Mater.* **13** 993
- [5] Geffroy P-M, Blond E, Richet N and Chartier T 2017 *Chem. Eng. Sci.* **162** 245
- [6] Takeda Y, Kanno R, Takada T, Yamamoto O, Takano M and Bando Y 1986 *Z. Anorg. Allg. Chem.* **540** 259
- [7] Rautama E-L and Karppinen M 2010 *J. Solid State Chem.* **183** 1102
- [8] Klimkowicz A, Cichy K, Chmaissem O, Dabrowski B, Poudel B, Świerczek K *et al* 2019 *J. Mater. Chem. A* **7** 2608
- [9] Motohashi T, Ueda T, Masubuchi Y, Takiguchi M, Setoyama T, Oshima K *et al* 2010 *Chem. Mater.* **22** 3192
- [10] Dasgupta T, Sumithra S and Umarji A M 2008 *Bull. Mater. Sci.* **31** 859
- [11] Narayanan A M and Umarji A M 2019 *J. Alloys Compd.* **803** 102
- [12] Lin Y S, MacLean D L and Zeng Y 2000 *High temperature adsorption process*, US Patent No. 6,059,858
- [13] Wu H-C and Lin Y S 2017 *Ind. Eng. Chem. Res.* **56** 6057
- [14] Narayanan A M, Parasuraman R and Umarji A M 2018 *Ind. Eng. Chem. Res.* **57** 14749
- [15] Jeon H, Choi W S, Biegalski M D, Folkman C M, Tung I-C, Fong D D *et al* 2013 *Nat. Mater.* **12** 1057
- [16] Reichmann M, Geffroy P-M, Richet N and Chartier T 2016 *J. Power Sources* **324** 774
- [17] Guntuka S, Farooq S and Rajendran A 2008 *Ind. Eng. Chem. Res.* **47** 163
- [18] Miura N, Ikeda H and Tsuchida A 2016 *Ind. Eng. Chem. Res.* **55** 3091
- [19] Ikeda H, Tsuchida A, Morita J and Miura N 2016 *Ind. Eng. Chem. Res.* **55** 6501
- [20] Beppu K, Hosokawa S, Shibano T, Demizu A, Kato K, Wada K *et al* 2017 *Phys. Chem. Chem. Phys.* **19** 14107
- [21] Ding H, Xu Y, Luo C, Wang Q, Li S, Cai G *et al* 2017 *Chem. Eng. J.* **323** 340
- [22] Nomura T, Zhu C, Sheng N, Murai R and Akiyama T 2015 *J. Alloys Compd.* **646** 900
- [23] West A R 2007 *Solid state chemistry and its applications* Student edn (New Delhi: Wiley India Pvt. Ltd.)
- [24] Rao C N R and Gopalakrishnan J 1997 *New directions in solid state chemistry* 2nd edn (Cambridge, UK: Cambridge University Press)
- [25] Jolivet J P, Henry M and Livage J 2000 *Metal oxide chemistry and synthesis: from solution to solid state* (Hoboken: Wiley-Blackwell)
- [26] Lee B and Pope E J A 1994 *Chemical processing of ceramics* (Hoboken, USA: Wiley)
- [27] Lee B and Komarneni S 2005 *Chemical processing of ceramics* 2nd edn (USA: CRC Press)
- [28] Peláiz-Barranco A, Guerra J D S, López-Noda R and Araújo E B 2008 *J. Phys. D: Appl. Phys.* **41** 215503
- [29] Patil K, Hegde M S, Rattan T and Aruna S T 2008 *Chemistry of nanocrystalline oxide materials: combustion synthesis, properties and applications* (Singapore: World Scientific)
- [30] Bezdicka P, Wattiaux A, Grenier J, Pouchard M and Hagenmuller P 1993 *Z. Anorg. Allg. Chem.* **619** 7
- [31] Wisgerhof E and Geus J W 1984 *Mater. Res. Bull.* **19** 1591
- [32] Toby B H and Von Dreele R B 2013 *J. Appl. Crystallogr.* **46** 544
- [33] Schneider C A, Rasband W S and Eliceiri K W 2012 *Nat. Methods* **9** 671
- [34] van der Pauw L J 1958 *Philips Res. Rep.* **13** 1
- [35] Muñoz A, de la Calle C, Alonso J A, Botta P M, Pardo V, Baldomir D *et al* 2008 *Phys. Rev. B* **78** 054404
- [36] Le Toquin R, Paulus W, Cousson A, Prestipino C and Lamberti C 2006 *J. Am. Chem. Soc.* **128** 13161
- [37] Hurst N W, Gentry S J, Jones A and McNicol B D 1982 *Catal. Rev.* **24** 233
- [38] Jin X, Wang J and Huang K 2017 *Solid State Ionics* **309** 48
- [39] Crumlin E J, Mutoro E, Liu Z, Grass M E, Biegalski M D, Lee Y-L *et al* 2012 *Energy Environ. Sci.* **5** 6081
- [40] Hess F and Yildiz B 2020 *Phys. Rev. Mater.* **4** 015801